Chapter 2
Fundamental Theories

2.1 Structures of Carbon Nanotubes

Carbon nanotubes can be considered as a hexagonal network of carbon atoms that has been rolled to make a seamless hollow cylinder. These hollow cylinders are tens micrometers in length but only about ten nanometers in diameters. Each end is capped with half fullerence molecule (Fig 2.1(a) [11]). A single-wall nanotube can be treated as a fundamental structure unit, which has a shell with only one atom in thickness. Such structure constitutes multi-wall nanotubes with multiple coaxial cylinders.

The tubes may belong to different symmetries because of the relation between the orientation of the graphite layer and the axis of the nanotube. The primary symmetry classification of a nanotube is either being achiral or chiral. Achiral tubes are a type of nanotubes that there is a mirror symmetry in its structure. Achiral nanotubes are classified into two kinds, armchair and zigzag nanotubes, as shown in fig 2.1(a) and (b) [11]. Chiral nanotubes exhibit a spiral symmetry but not a mirror one.

The chiral vector, as shown in fig. 2.2(a), can specify the structures of the nanotubes. Equation is listed below, with n and m being positive integers and m being less than n.

$$Ch=na_1+ma_2(n,m)$$

Armchair nanotubes correspond to the case of n=m; that is, Ch=(n,n). Zigzag nanotubes correspond to the case of m=0, or Ch=(n,0). Other (n,m) chiral vectors correspond to chiral nanotubes. The diameter of the carbon nanotube, D_t, is L/π, in which L is the circumferential length of the nanotube:

$$D_t= L/\pi, L=\mid C_h \mid=(C_h)^{1/2}=a(n^2+m^2+nm)^{1/2}$$

The chiral angle θ is defined as the angle between the vectors C_h and a_1, with the values of the
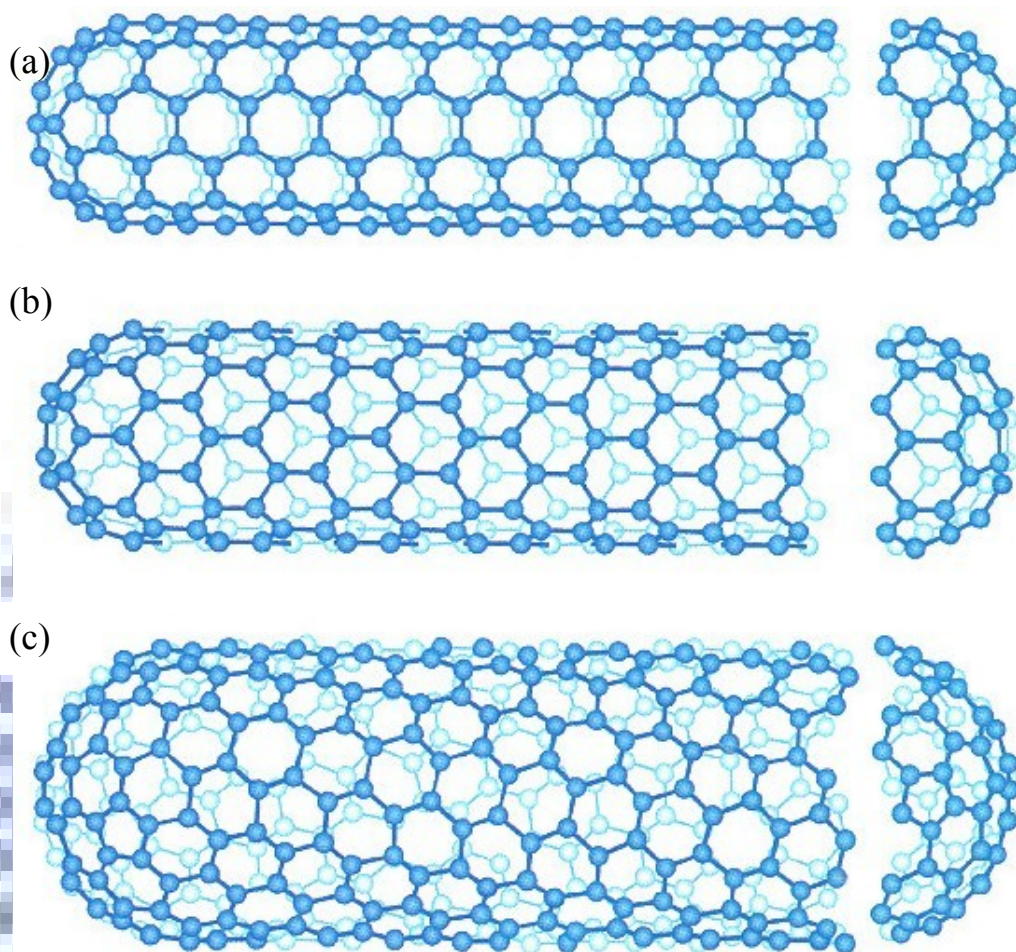
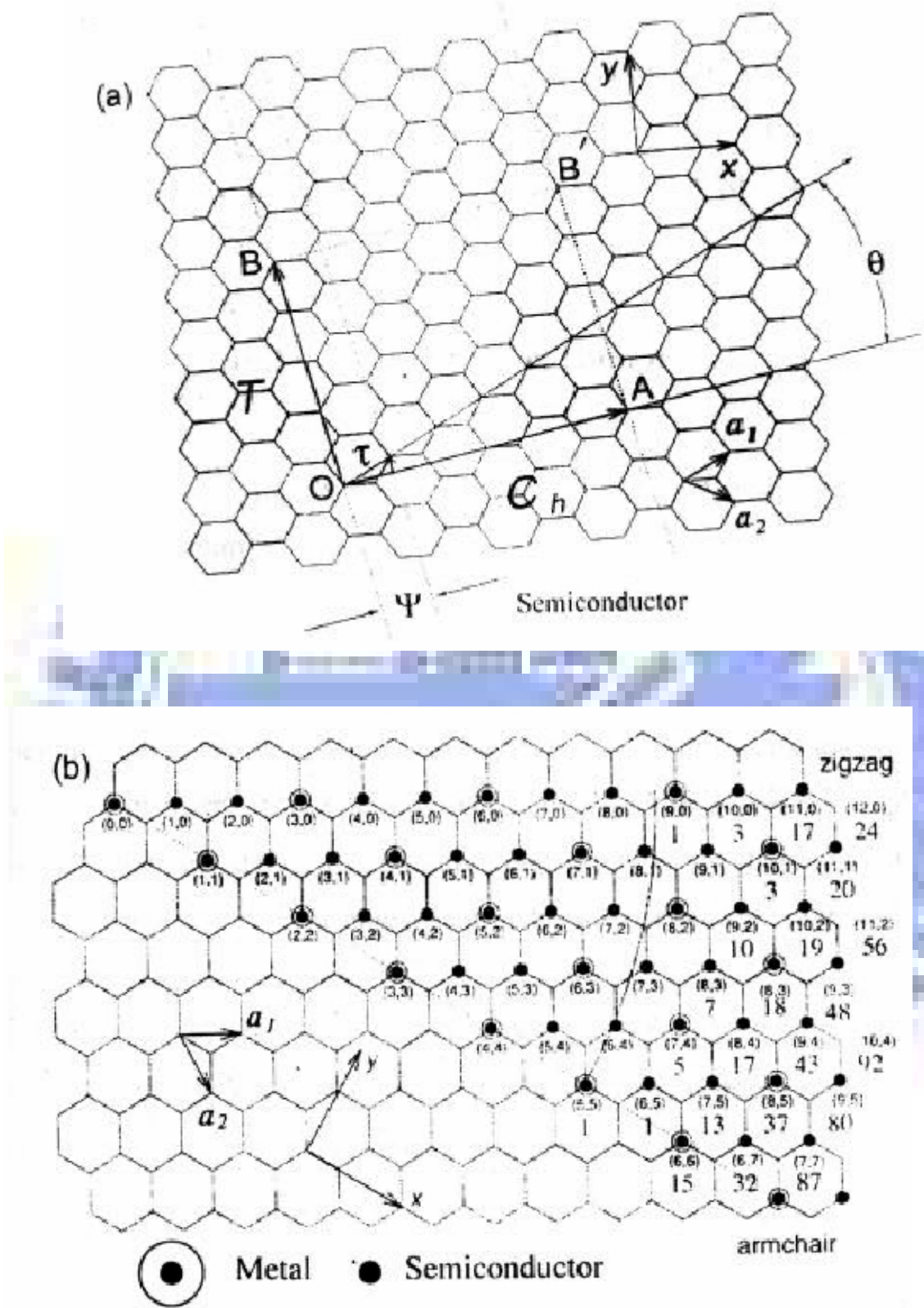**Fig. 2.1 (a) an "armchair" tubule, (b) a "zigzag" tubule, and (c) a "chiral" tubule [11].**

Fig. 2.2 (a) The chiral vector OA is defined on the honeycomb lattice of carbon atoms by unit vectors a₁, a₂ and the chiral angle è with respect to the zigzag axis. (b) Possible vectors specified by the pairs of integers (n,m) for general carbon tubules, including zigzag, armchair, and chiral tubules [11].

range $0 \leqq |\theta| \leqq 30$, because of the hexagonal symmetry of the honeycomb lattice.

The electric features of SWNTs were predicted theoretically in 1992. Hamada [7] and Satio [8] observed that carbon nanotubes can be either metal or semiconductor in electric conductivity, which is determined by the condition below.

n-m=3q, q=0   small band gap semiconductor

n-m=3q   semiconductor

n-m=0   metal

The prediction was supported by Wildoer [9,10]. Fig. 2.2(b) shows how the helicity of carbon nanotubes affects the electric properties.
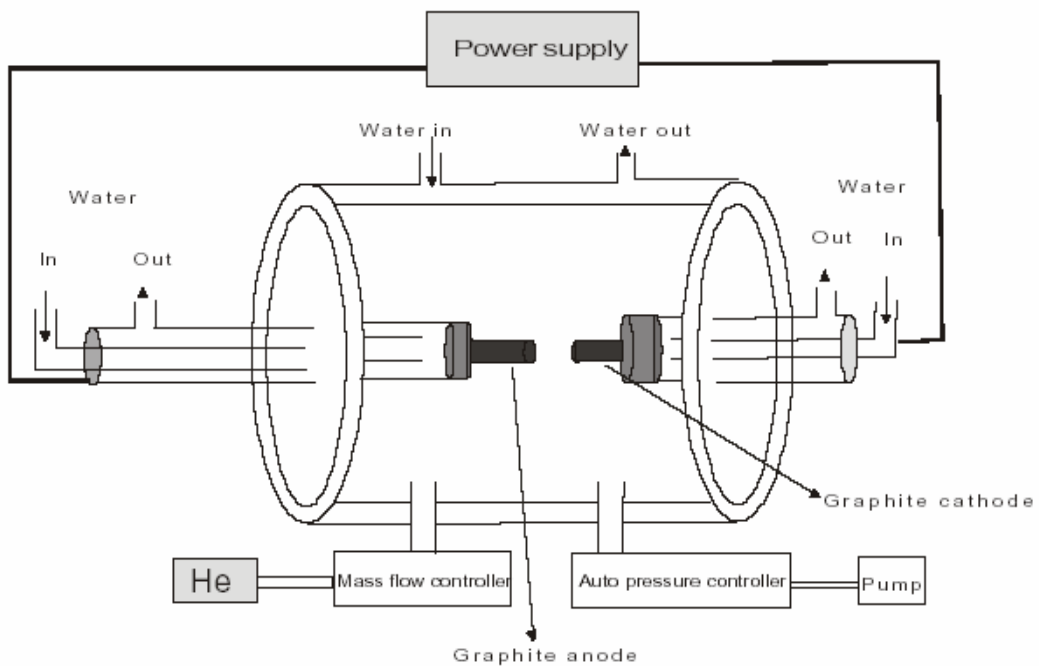
2.2 The Methods of Carbon Nanotubes Synthesis

To synthesize carbon nanotubes, researchers employ three main categories: arc discharge with metal in the rod or not, laser vaporization with the metal-graphite composite target, and carbon monoxide decomposition or hydrocarbon pyrolysis by using the metal catalyst generally.

2.2.1 Arc-Discharge Methods

The arc-discharge method for the preparation of carbon nanotubes is similar to that used for the synthesis of fullerenes [12,13]. The arc discharge experiments are performed in a stainless steel chamber in which helium gas was filled under the pressure ranging from 10 to 500 Torr. A dc (direct current) voltage of about 30 V is applied between two graphite rods (one 5 mm and the other 13mm in diameter). The thin rod is connected to the positive of a dc power supply, the thick rod to the negative. When the rods were brought close, discharge was ignited, resulting in the formation of plasma. The current of plasma varied from 40 to 100A. As the thin rod (positive electrode) was consumed, it was fed to keep the gap distance between the electrodes about 1mm as in fig. 2.3 [14]. On the thicker rod (negative electrode),

carbonaceous deposit was formed. When the metal catalyst is to be used, a hole is drilled in the carbon anode and filled with the mixture of metal and graphite powder. In this case, most nanotubes are found in the soot deposited on the arc-chamber wall. It is important to note that the obtained materials consist of not only nanotubes but also nanoparticles, fullerenes and a lot of amorphous carbon. Ebbesn [15] reported that open tubes can be obtained by oxidizing the deposit. However, only 1 wt% of the initial deposit remains after oxidation. From previous work [16], CH_4 and H_2 were better than inert gases for the production of MWNTs. Using CH_4 and H_2, the researchers gained high yield of carbon nanotubes and low proportion of co-existing carbon nanoparticles.


Fig. 2.3 Schematic illustration of the arc-discharge system [14].

2.2.2 Laser Vaporization

Guo et al., [17] invented a new method for synthesizing single-walled nanotubes (SWNT) in which carbons were vaporized by laser impinging on the metal-graphite composite target.

In contrast to the arc method, direct vaporization is controllable on the growth condition and produces nanotubes in higher yield (70-90%) and quality. SWNTs are about 1 nm in diameter and are arranged in bundles. No amorphous carbon coating on the tubes is observed.

The oven laser-vaporization apparatus [18] (Fig. 2.4) is used to produce fullerenes and MWNTs. Scanning laser beam is focused to a 6-7 mm diameter spot onto the metal-graphite composite target. The laser beam scans across the target surface under computer control to maintain a smooth, uniform face for vaporization. The target is supported by graphite poles in an 1 inch quartz tube evacuated to 10 mm and then filled with 500 Torr argon flowing at 50 sccm. The flow tube is mounted in a high-temperature furnace, with a maximum temperature of 1200 ℃. The soot produced by the laser vaporization is swept by the flowing gas from the high temperature zone, and deposited into a water-cooled copper collector positioned downstream.
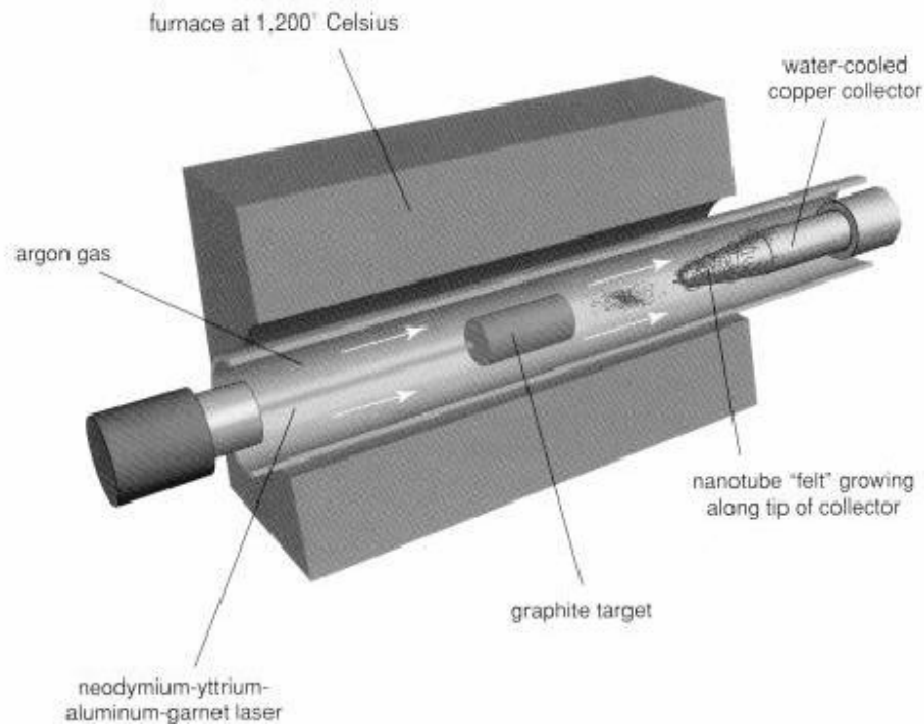
Fig. 2.4 Oven laser-vaporization apparatus [18].
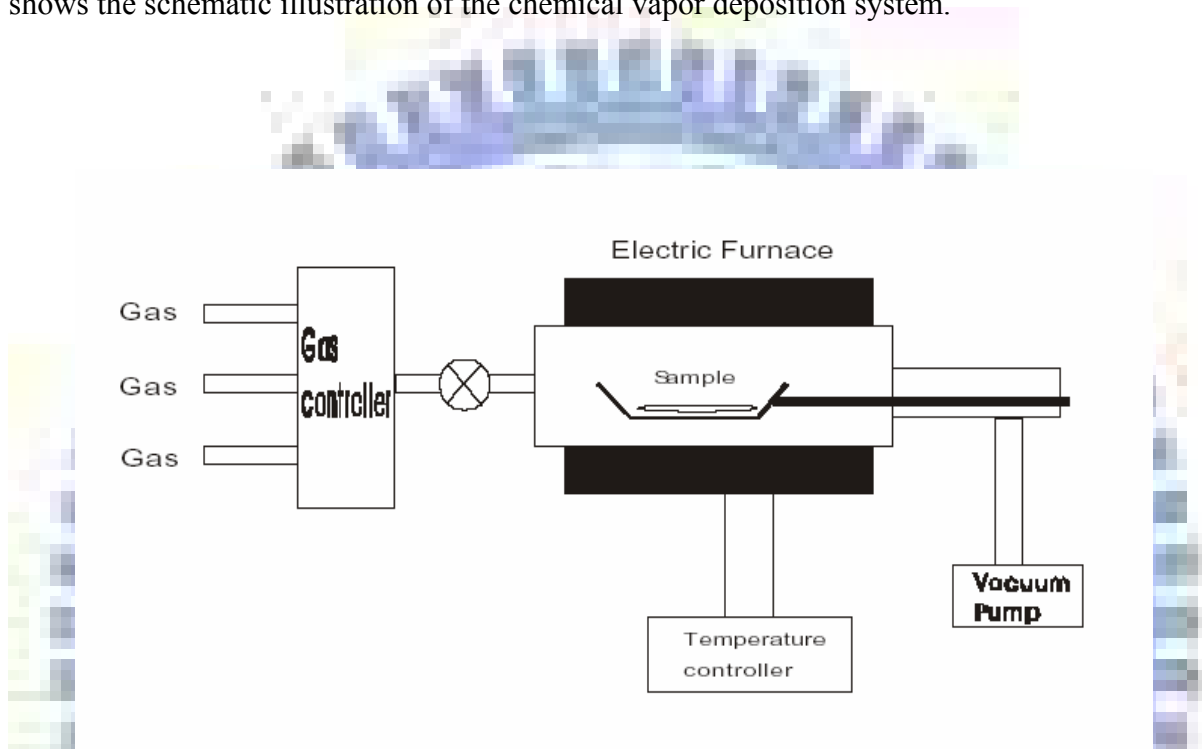
2.2.3 Chemical Vapor Deposition

Chemical vapor deposition technique deals with gas phase system in carbon nanotubes are formed by the deposition of carbon-containing gas [19]. The gas phase techniques are amenable to continuous process since the carbon source is continually replaced by flowing gas. In addition, the final purity of carbon nanotubes can be quite high enough to minimize purification steps. The advantage of chemical vapor deposition technique is that carbon nanotubes can be synthesized continually and thus the growing pure carbon nanotubes could be obtained in the optimum condition. That is a very good way to synthesize large quantities of carbon nanotubes under relatively controlled conditions. So the chemical vapor deposition has advantages for scale-up and commercial productions.

Nikolaev et al., [20] reported that the high-yield single-walled carbon nanotubes were obtained at high temperature and high pressure (1200℃, 10 atm) with carbon monoxide as carbon source. Smalley et al. [21] refined the process to produce large quantities of single-walled carbon nanotubes with remarkable purity. High pressure conversion of carbon monoxide has to be commercialized by Nanotechnologies Inc (Houston, TX) for large scale production of high purity single-walled carbon nanotubes. Transition metal (e.g. Fe, Co, Ni) particles are known to be catalysts for vapor grown carbon nanotubes synthesis, in which hydrocarbons (e.g., CH_4, C_6H_6) are used as gas source. Metal catalysts are generally necessary to activate carbon nanotubes growth. A variety of other catalysts, hydrocarbons and catalyst supports have been used successfully by various groups the world wide to synthesize carbon nanotubes [22, 23].

Nikolaev and co-workers [20] reported that hydrocarbon pyrolize readily on surfaces heated above 600-700 ℃. Carbon nanotubes growth with hydrocarbons has substantial amorphous carbon deposited on the surface of tubes and requires further purification. Even though the disassociation of hydrocarbons at low temperature affects the purity of carbon nanotubes, but the low processing temperature enables the growth of carbon nanotubes on a

variety substrates.

The synthesis of well-aligned straight carbon nanotubes on a variety of substrates has been accomplished by the use of plasma enhanced chemical vapor deposition (PECVD) where the plasma is excited by a microwave source [24,25,26] or a DC source [27]. Fig. 2.5 shows the schematic illustration of the chemical vapor deposition system.

Fig. 2.5 Schematic illustration of the chemical vapor deposition (CVD) system.

2.3 The Application of Carbon Nanotubes

Since the miniaturization of devices have been continuous, computers become faster and smaller. Meanwhile silicon has become popular device material due to its physical and geological abundance. The size of device is halved every 3 years. The trend of semiconductor device feature size will be reduced continuously. In order to overcome this technological limit of the nanometer scale materials, carbon nanotubes have attracted interest in semiconductor technology and scientific field. Relative research fever and the development s of commercial applications such as hydrogen storage, atomic force microscope probe, microelectronic

transistor, electrical field emitter of flat panel display and scanning tunneling microscope tip have been stimulated tremendously.

2.3.1 Transistors

The field-effect transistor – a three-terminal switching device – can be constructed of only one semi-conducting SWNT [28]. By applying a voltage to a gate electrode, the nanotube can be switched from a conducting to an insulating state. A schematic representation of such a transistor is given in fig. 2.6. Such carbon nanotube transistors can be coupled together, working as a logical switch, which is the basic component of computers.
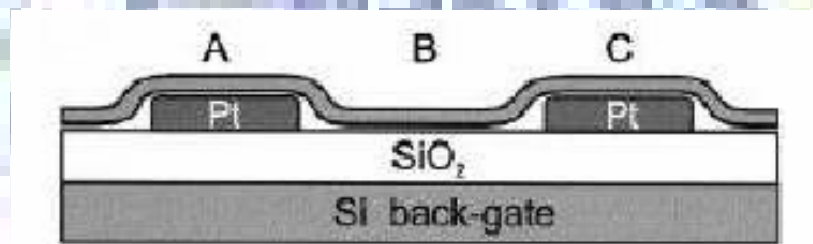
Fig. 2.6 A single semi-conducting nanotube is contacted by two electrodes. The Si substrate, which is covered by a layer of SiO_2 300nmthick, acts as a back-gate [61].

2.3.2 Atomic Force Microscope, AFM

Carbon nanotubes have been expected to be promising probes for various types of scanning probe microscopes (SPM) because they have the unique physical properties.

Dai and coworkers [29] demonstrated that high aspect ratio of the carbon nanotubes enables us to observe deep hole which cannot be detected by conventional tip. Carbon nanotubes tips were applied to non-contact atomic force microscopy and a clear image of deoxyribonucleic acid (DNA) helical turn by making the best of sharpness of the carbon

nanotube tip apex, as investigated by Uchihashi et al [30].

Jarvis and coworkers [31] applied carbon nanotubes probes to detect salvation forces in water by atomic force microscope (AFM). Carbon nanotube was attached tungsten tips for scanning tunneling microscopy (STM) by Ishikawa [32].

Ishikawa et al., have studied the application of carbon nanotubes probe for the measurement of friction using the AFM [33]. They concluded that the friction versus load curve using the unique carbon nanotube tip shows the behavior different from conventional tip and strong scanning length dependency of the friction force is found due to the deformation of carbon nanotube. Fig. 2.7 shows the carbon nanotube tip was used as probe on atomic force microscope.
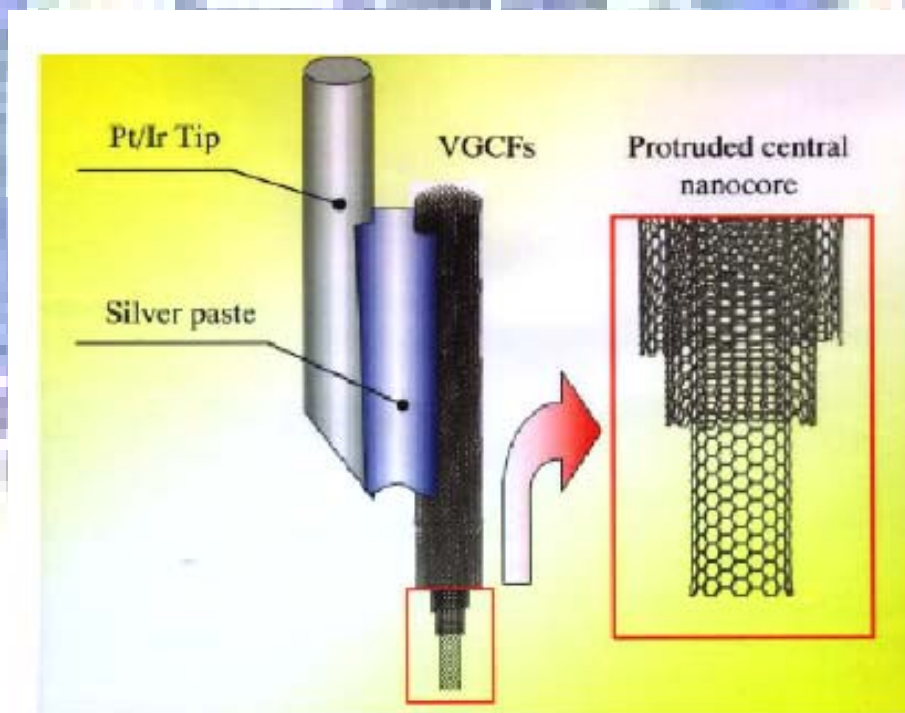
Fig. 2.7 Use of a MWNT as AFM tip. VGCF stands for Vapour Grown Carbon Fiber. At the centre of this fiber the MWNT forms the tip [62].

2.3.3 Field Emission Display, FED

Carbon nanotubes have been demonstrated to possess remarkable mechanical and electric properties for field emission application [34,35]. Fig. 2.8 shows the structure of one form of FED based on emission of electrons from sharp-tipped cones. Vertical alignment carbon nanotubes have excellent electron emission properties. A powerful application of electronic emission sources can be expanded to flat panel displays such as field emission display (FED). The application of carbon nanotubes to field emission displays requires their vertical alignment on cathode electrodes for better emission. Choi et al. [36], a Korean team of Samsung, have prepared a full color display based on carbon nanotubes electronic sources. The vertically aligned carbon nanotubes were fabricated by an arc-discharge method. They mixed a conglomeration of single-walled carbon nanotubes pasted on glass. In order to simplify the process, it is desirable to grow carbon nanotubes on cathode with well alignment. Many researchers investigated the direct growth alignment carbon nanotubes methods which are compatible with current silicon fabrication techniques for electronic application. Kind et al [37] synthesized well-aligned carbon nanotubes on silicon wafer using micro contact printing of catalysts. However, it is still a challenge to directly fabricate the carbon nanotubes field emission for commercial application. Zhang et al. [38] investigated the fabrication of vertically aligned carbon nanotubes patterns by chemical vapor deposition for field emitters. Table 2.1 compared field emission property of carbon nanotubes with other materials.
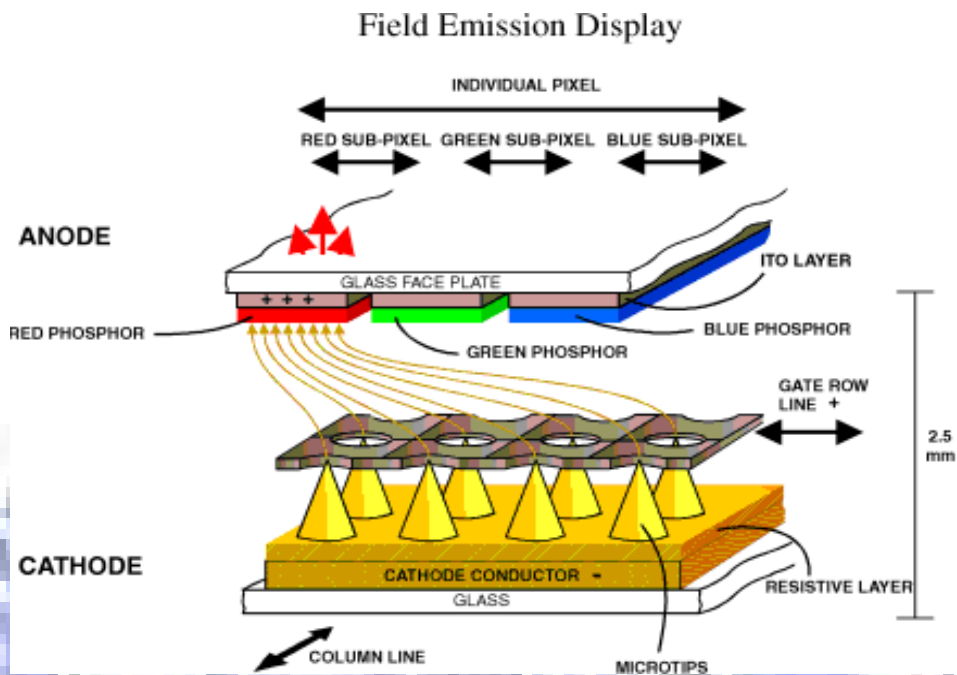
Field Emission Display

Fig. 2.8 Schematic diagram of a field emission cell.

Emitter	Eto(V/μm; 0.01mA/cm2)	1mA/cm2 (V/μm)	10 mA/cm2 (V/μm)
Mo tips			50-100
Si tips			50-100
Diamond	24		40
Diamond B doped	16		30
Diamond Cs coated	10		28
Diamond N doped	1.5		>>8
Graphite powder(<1μm)			17
Amorphous carbon	4		~50
Nanostructured diamond	1-2	~3	5
Carbon nanotubes			
95, de Heer, arc, aligned	4		6.5
97, Wang, arc, O2 plasma	0.8	3	
98, Bonard, arc	2.6		4.6
98, Chen, HFCVD, aligned nanofiber, 50-100 nm	2.7	>>6.5	
98, Bonard, arc, single-walled	2.8		5.2
99, Dai, CVD, aligned, 16 nm	0.8-1.2	2.7-3.3	4.8-5.3
99, Xu, CVD, 20nm	4.7	5.8	6.5
99, MER Corp., arc, 7-12 nm ta-C coated	2.4 1.5		
99, Xu, CVD, aligned, 10-30 nm	3.2	4.6	
99, Zhu, laser, single-walled			4-7
nanofiber(38), MPECVD, 60-80 nm	2.7		
aligned nanotube（38）, MPECVD, ~100 nm	1.8	3.2	~4.4

Table 2.1 Field emission properties of carbon nanotubes compared with other materials.

2.4 Theory of Field Emission

2.4.1 Field Emission from Metals

Field emission is a quantum-mechanical phenomenon in which electrons tunnel through a potential barrier at the surface of a solid as a result of the application of a large electric field. Field emission is distinct from thermionic emission and photoemission in which electrons acquire sufficient energy via heating or energy exchange with photons, respectively, to overcome (go over) the potential barrier. In field emission external electric field on the order of 10^7 V-cm^{-1} is required for appreciable electron currents. The presence of the electric field makes the width of the potential barrier finite and therefore permeable to the electrons. This can be seen with the help of fig. 2.9 which presents a diagram of the electron potential energy at the surface of a metal.

The dashed line in fig. 2.9 shows the shape of the barrier in the absence of an external electric field. The height of the barrier is equal to the work function of the metal, φ, which is defined as the energy required removing an electron from the Fermi level E_F of the metal to a rest position just outside the material (the vacuum level). The solid line in fig. 2.9 corresponds to the shape of the barrier in the presence of the external electric field. As can be seen, in addition to the barrier becoming triangular in shape, the height of the barrier in the presence of the electric field E is smaller, with the lowering given by [39]

$$\Delta\phi = \left(\frac{eE}{4\pi\varepsilon_0} \right)^{1/2} \tag{2.1}$$

where e is the elementary charge and ε_0 is the permittivity of vacuum.

Knowing the shape of the energy barrier, one can calculate the probability of an electron with a given energy tunneling through the barrier. Integrating the probability function multiplied by an electron supply function in the available range of electron energies leads to an expression for the tunneling current density J as a function of the external electric field E. The tunneling current density can be expressed by Eq. (2.2) which is often referred to as the

Fowler-Nordheim equation [41,42]

$$J = \frac{e^3 E^2}{8\pi h \phi t^2(y)} \exp\left[\frac{-8\pi(2m)^{1/2}\phi^{3/2}}{3heE} v(y)\right] \tag{2.2}$$

where $y=\Delta\varphi/\varphi$ with $\Delta\varphi$ given by Eq. (2.1), h is the Planck's constant, m is the electron mass, and $t(y)$ and $v(y)$ are the Nordheim elliptic functions; to the first approximation $t^2(y)=1.1$ and $v(y)=0.95 - y^2$. Substituting these approximations in Eq. (2.2), together with Eq. (2.1) for y and values for the fundamental constants, one obtains

$$J = 1.42\times10^{-6} \frac{E^2}{\phi} \exp\left(\frac{10.4}{\phi^{1/2}}\right) \exp\left(\frac{-6.44\times10^7 \phi^{3/2}}{E}\right) \tag{2.3}$$

where J is in units of A cm^{-2}, E is in units of V cm^{-1} and φ in units of eV. Plotting log (J/E^2) vs. 1/E results in a straight line with the slope proportional to the work function value, φ, to the 3/2 power. Eq. (2.3) applies strictly to temperature equal to 0°K. However, it can be shown that the error involved in the use of the equation for moderate temperatures (300°K) is negligible [42].

2.4.2 Field Emission Form Semiconductors

To a large degree, the theory for electron emission from semiconductors can be derived parallel to the theory for metals. However, special effects are associated with semiconductors due to the state of their surface and the fact that an external field applied to a semiconductor may penetrate to a significant distance into the interior. The classic theoretical treatment of electron emission from semiconductors is given in Ref. [43]. For the case when the external electric field penetrates into the interior of an n-type semiconductor and the surface states are neglected, log(J/E^2) is shown to be a linear function of 1/E. However, in place of the work function φ in the Fowler-Nordheim equation one needs to substitute a quantity χ-δ, where χ is the electron affinity defined as the energy required for removing an electron from the bottom of the conduction band of the semiconductor to a rest position in the vacuum, and δ denotes

the band bending below the Fermi level. These parameters are illustrated in fig. 2.10. The linear dependence of $\log(J/E^2)$ on $1/E$ is expected only if the density of the current flowing through the sample is much smaller than the current limiting density $J_{lim} = en\mu_n E/\varepsilon$, where μ_n is the electron mobility and n is the electron concentration in the bulk of the semiconductor [44,45]. At $J \approx J_{lim}$, the Fowler-Nordheim character of the relationship $J(E)$ passes into the Ohm's law (if the dependence of electron mobility on the electric field is neglected) which results in the appearance of the saturation region in the emission current vs. voltage curve [46]. Such saturation regions were observed experimentally for lightly doped n-type semiconductors and for p-type semiconductors [47,48]. Electron emission from semiconductors has been a subject of more recent theoretical considerations which takes into account complications due to electron scattering, surface state density, temperature, and tip curvature [49,50,51].

2.4.3 Fowler-Nordheim equation for a single-cell gated FEA

Fig. 2.11 shows a schematic diagram of a cell in a micro-fabricated gated FEA. The emitter has the form of a sharp tip so that advantage can be taken of the well-known enhancement of electric field at surfaces exhibiting high curvature. If voltage V_g is applied to the gate electrode, the electric field E at the tip is given by Eq. (2.4)

$$E = \beta \times V \tag{2.4}$$

where the proportionality constant β is called the field enhancement or field conversion factor. If E is in units of V cm^{-1} and V_g is in units of V, β is in units of cm^{-1}. If the area from which emission of electrons takes place is denoted as α, and Eq. (2.4) is substituted for E in the Fowler-Nordheim equation Eq. (2.3), the following expression is obtained

$$I = J \times \alpha = A \times V_g^2 \exp\left(- B / V_g\right) \tag{2.5}$$

where

$$A = 1.42 \times 10^{-6} \times \alpha \times \beta^2 / \phi \times \exp\left(10.4 / \phi^{1/2}\right) \qquad (2.6)$$

and

$$B = 6.44 \times 10^7 \times \phi^{3/2} / \beta \qquad (2.7)$$

In Eq. (2.5) I is in units of A, α in units of cm^2, β in units of cm^{-1}, ϕ in units of eV and V_g in units of V.

Plotting experimental values of electron emission current vs. gate voltage in the so-called Fowler-Nordheim coordinates, $\ln (I/V_g^2)$ vs. $1/V_g$, is a common way of analyzing electrical performance data for gated field emitter arrays. As can be seen from Eq. (2.5), such a plot will appear as a straight line over a large portion of the emission region. The constants A and B in Eq. (2.5) provide a way of comparing performance of FEAs with different geometrical parameters, emitter materials, etc. over a wide range of emission currents. The A and B values can be extracted from the least-squares fit to experimental data with A related to the intercept and B to the slope of the straight line in the Fowler-Nordheim coordinates.
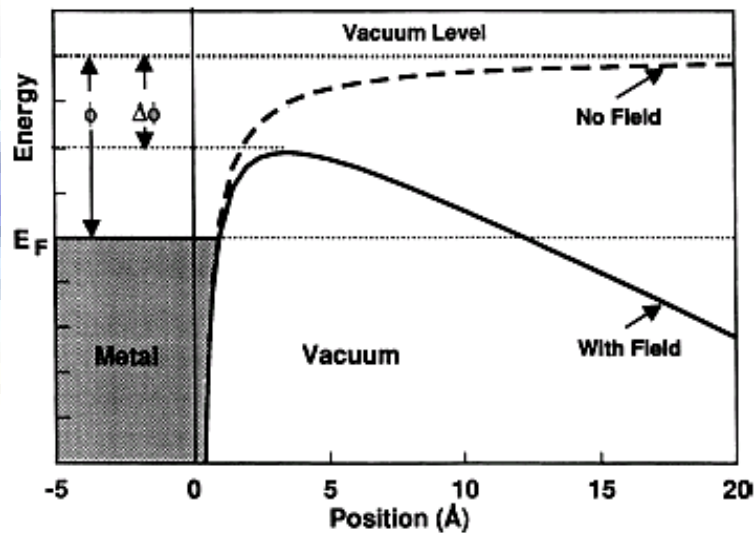
Fig. 2.9 Diagram of potential energy of electrons at the surface of a metal.
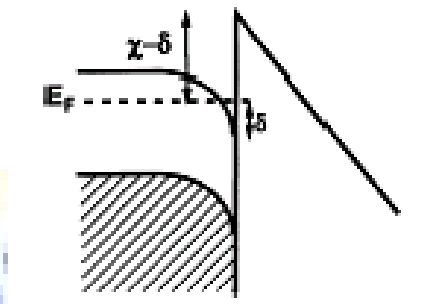
Fig. 2.10 Diagram of the potential energy of electrons at the surface of an n-type semiconductor with field penetration into the semiconductor interior.
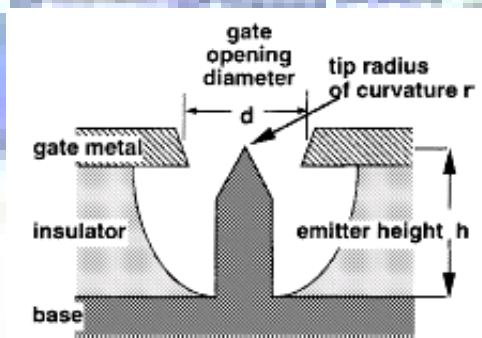
Fig. 2.11 Schematic diagram of a cell in a FEA. The emitter height is denoted by h, the gate aperture diameter by d, and the tip curvature by r.